Behavior of a Composite Steel Decking and Boarding System in Fire Based on Large-Scale Experimental Testing and Numerical Modelling

Jaleel Claasen and Antonio Cicione, Department of Civil Engineering, Stellenbosch University, Stellenbosch, South Africa

Dirk Streicher, Department of Civil Engineering, Stellenbosch University, Stellenbosch, South Africa and Ignis Testing, Cape Town, South Africa

Richard Walls ⓘ*, Department of Civil Engineering, Stellenbosch University, Stellenbosch, South Africa

Abstract. This paper presents experimental and numerical results of an investigation into the thermal and structural behaviour of an innovative modular structural steel system, which includes cellular beams, that was tested in a 1-h standard fire scenario while loaded. The modular system consists of a 5.66 × 3.8 m rectangular steel frame, with a profiled steel sandwich decking (SD) system attached, which comprises of (a) profiled steel decking, (b) fibre cement, and (c) calcium silicate boards and strips. The SD system is suspended from the underside of the horizontal structural members to provide inherent fire protection to the steel beams from the bottom and acts as the load-bearing component of the flooring. The purpose of the experiment was to determine the fire resistance of the structural system, whilst under load, which is primarily based on the fire resistance of the SD system. Temperature data for the SD system was collected during the experiment and used to validate a numerical finite element analysis model. This study shows that the SD system was able to achieve a fire resistance rating of 57 min in the experiment which was governed by insulation resistance. A lower fire resistance rating is estimated based on numerical models. Structural resistance was maintained throughout the test. During preliminary testing structural collapse was observed in a separate experiment which highlights how the system is sensitive to damage to the ceiling boards. Numerical results highlight that thermal bowing and movement may result in changes in thermal interactions between adjacent elements. This paper provides novel large-scale experimental data on a loaded flooring system in fire.

Keywords: Sandwiched decking, Finite element model, Cellular beams, Fire resistance, Structural steelwork, Passive protection, Large-scale tests

---

*Correspondence should be addressed to: ; Richard Walls, E-mail: rwalls@sun.ac.za

1. Introduction

The use of profiled steel sheet dry board (PSSDB) composite flooring systems was first proposed by [1] as a replacement to existing timber joist floors in construction. PSSDB composite panel systems are essentially a lightweight composite structure composed of a profiled steel sheet and dry boards which are assembled with a series of screws. The sandwich decking (SD) system tested in this work is a variation of a PSSDB composite flooring system. Studies on the performance and implications of PSSDB systems to be used as flooring, walling, and roofing systems in construction have been performed in the past by various researchers [2–6]. In the past years there has been extensive research on steel structures in fire, gaining impetus from some of the original large-scale tests at Cardington [7], with growing numbers of studies on numerical modelling [8–10], the development of design guidelines [11, 12] including the production of composite design models [13, 14]. An overview of large-scale studies is provided by Bisby et al. [15, 16]. However, various critiques on standard fire testing have been published highlighting shortcomings, and failure mechanisms not identified [17]. Of importance is that when testing single elements in a standard fire test, global failure mechanisms involving the interaction of structural elements is typically not identified.

While numerous studies have been conducted into the fire resistance performance of light gauge steel frame (LSF) systems [18–22], limited research has been conducted on the fire resistance performance of profiled steel sheet decking boarding systems (i.e. when there is a continuous steel sheeting system between boards rather than distinct studs/beams). The studies into the performance of LSF system lined with insulating materials have provided significant insights into the fire resistance performance of light-weight structural systems and the insulating materials used. However, no direct comparisons of profiled steel sheet decking boarding systems can be made to LSF system as these systems tend to vary with regards to the type and configuration of insulating materials used and structural framing layouts. Systems need to be investigated on a case-to-case basis. Hence, for the SD system in this work to be introduced as a lightweight, quick assembly, fire-rated flooring system into the construction industry, a proper investigation into the behaviour at elevated temperatures needs to be carried out through experimental testing and numerical modelling.

The experimental frame tested in this work is based on the design of a single module (see Fig. 1) of the cellular beam modular office building system, referred to as the Cellular beam structural (CBS) system, that was originally proposed by the Southern African institute of steel construction (SAISC). The steelwork is protected by the SD flooring system suspended from the underside of the beams. Previous studies have been performed to assess the fire resistance of the CBS system. The first study investigated the thermal behaviour of the CBS system [23, 24], and the other focused on the structural behaviour of the CBS system in fire [25, 26]. Small-scale experiments were conducted by Marx [23, 24] on the SD system (i.e. only the sandwich system without steel beams to investigate the heat transfer through the various layers of the flooring components). The Marx study used the experimental results to develop and benchmark thermal response models of the
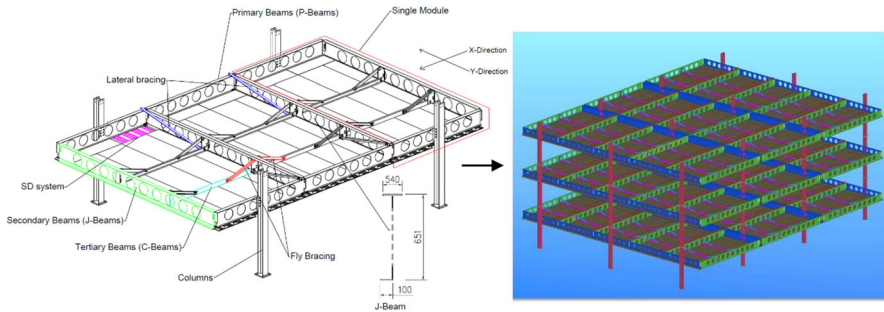
Figure. 1. The modular cellular beam structural system (CBS) showing both a single sub-structure (i.e., three interconnected modules) and an entire building.

SD system, which, in turn, was used to develop numerical models that can predict the temperature evolutions of the horizontal steel members. Kloos [25, 26] used the numerical data produced by Marx [23, 24] to develop numerical thermal-stress models of the CBS structural members. The numerical models produced by the aforementioned research studies culminated in a fully de-coupled thermomechanical analysis of the CBS system.

However, due to the limited size of the tested samples (430× 340 mm), the experiments did not fully capture the thermal behaviour of the SD system. Shortcomings that this work address are (a) the dehydration reactions that occur within the calcium silicate (CSB) and fibre cement (FCB) boards at elevated temperatures are included and captured, (b) movement of the system during full-scale testing is considered, which can be associated with cracking of boards, (c) samples are loaded during experiments, (d) joints between boards have been included (and samples often fail at joints in fire tests), and (e) the influence of the system on steel temperatures has been considered. Understanding the dehydration reactions that occur within the boarding materials is key as this tends to have a significant influence on the overall fire resistance performance of the system, especially with regards to the CSB. Furthermore, the temperature evolutions of the horizontal structural steel members were predicted entirely through numerical modelling without any experimental data to benchmark against. As the system deflects and cracks, delamination, buckling and other phenomena can compromise the performance.

The work in this paper was carried out to further investigate the thermal behaviour of the SD of the CBS system and quantify the fire resistance. The work consists of a large-scale furnace test (5.66×3.8 m steel frame with SD system attached) in addition to the development of a finite element model. Experimental data from the investigation is first presented, followed by the development of a numerical model in Abaqus. Results are then presented along with discussions and conclusions. Data associated with this paper, including technical drawings, temperature data and detail of numerical models can be found at [27] in an associated online repository. Reference [28] is a thesis in which the work was originally derived and provides extended discussions on all aspects addressed. A detailed
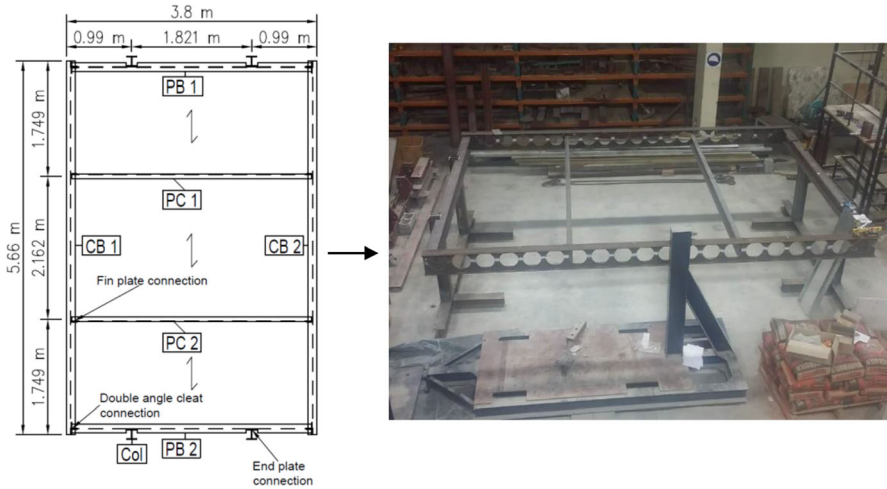
Figure. 2. **Experimental frame layout and structural components terminology.**

thermal-stress analysis of the experimental frame (see Fig. 2) is presented in [29]. Hence, this paper is the first journal article focussing specifically on the SD flooring system.

After some minor modification the proposed SD presented in this work will provide a novel, lightweight, trafficable, 60-min fire rated flooring system. This type of system can be assembled off-site, transported by truck, and installed onsite by unskilled labour. The lightweight nature of the system, in addition to no wet trade being involved, results in no formwork being needed and less reliance on heavy equipment (e.g., cranes) on site. These attributes of the SD system could result in a more effective construction process, which, in turn, would result in earlier completion and occupation. Hence, it will be beneficial for construction of a variety of buildings, and not only for use in the cellular beam structure presented in this work. Challenges associated with the system include acoustic performance, and ensuring that the fire resistance can be achieved, as addressed in this paper.

2. Experimental Setup

Two tests of the same size were undertaken as part of this work, (1) a main large-scale test and (2) a preliminary calibration test of just the ceiling system. The large-scale test, which forms the basis of this paper, was conducted with a newly built furnace at the Ignis Testing facility [30] located in Cape Town, South Africa. The preliminary calibration test was conducted to highlight potential failure mechanisms and ensure the furnace functioned correctly. The inner dimensions of the furnace were 6 ×4 ×1.185 m (L ×W× H). The experimental structural frame was designed to be independent from the furnace walls with an approximate gap of 100 mm between the horizontal structural elements and the furnace walls.
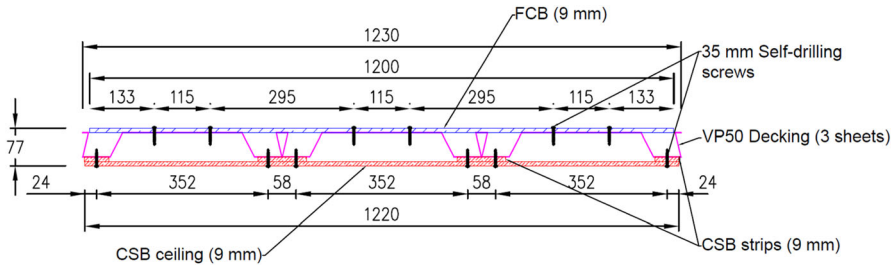
Figure. 3. SD system cross-sectional view showing the top fibre cement board (FCB), decking (VP50) and calcium silicate board ceiling (CSB) (units in mm).

The test was done according to SANS 10177-2 [31], which is based on the ISO 834 requirements and time–temperature curve. The three pass/fail criteria, which are as per Eurocode specifications, are (a) integrity (no smoke and flame to penetrate the system), (b) insulation (unexposed face temperature increase limited to 180°C above ambient at any point, with the average temperature increased limited to 140°C above ambient), and (c) structural resistance (i.e. load can be carried). Two 300 kW diesel burners were used to heat the furnace (see Fig. 3). The average furnace temperature was measured using six plate thermocouples positioned inside the furnace all round to control the burners and to assess if the ISO 834 standard fire curve was achieved during testing.

2.1. Experimental Frame

The experimental frame (see Fig. 2) used consists of ten main structural elements made of grade S355 steel. The horizontal structural components consisted of: (a) two $203 \times 133 \times 25$ UB primary beams spanning 3.64 m; (b) two $285 \times 133/133 \times 25$ symmetrical secondary cellular beams connected to the primary beams, spanning 5.66 m, and (c) two PC180 × 70 channel beams connected to the secondary beams. The SD is connected to and spans between the primary and channel beams. Two columns, consisting of $152 \times 152 \times 23$ UC sections, were attached to each of the primary beams with a footing system attached to the bottom of the columns. For more details on the structural layout and elements used in the experimental frame, the reader is referred to a recent work which focussed on a detailed study of the steelwork system presented in this paper [29].

2.2. Sandwich Decking (SD) System Components and Attachment

The SD system attached to the experimental frame consisted of Voidcon VP50 profiled steel sheeting with fibre cement boards (FCB) attached (9 mm) to the top and calcium silicate boards (9 mm) and calcium silicate board strips (9× 100 mm) attached to the bottom. Promatec-H boards from Marley Building Systems (now trading as Etex South Africa) was used for these. The fibre cement board was attached to the top using pairs of 35 mm self-drilling screws spaced 115 mm apart and spaced at 200 mm longitudinally along the top flute section of the steel deck-

ing. The calcium silicate boards (CSB) are used for the ceiling, along with CSB fixing strips, and are attached using pairs of 35 mm self-drilling screws spaced 58 mm apart and 200 mm in the longitudinal direction along the bottom trough section of the steel decking. Figure 3 depicts a representative section of the SD system which includes a single FCB and CSB, and three interlocked VP50 profiled steel sheets. The SD spans between supporting steel members, and the three components of it act compositely. Furthermore, the SD system is classified according to the size of the profiled steel decking and fibre cement board thickness used, hence, the SD system tested in this work is referred to as the VP50-9 SD system. For ambient temperature structural tests on a variety of SD configurations (i.e. different board and decking specifications) refer to [28].

The VP50 decking was first laid on top of 100×10 mm steel plates hung from the underside of the primary and tertiary support beams using hanger bolts as depicted in Fig. 4a, thus sandwiching the steel decking between the steel plates and support beams. The 10 mm thick steel plates are approximately the same thickness as the calcium silicate board strips used when attaching the CSB and are located in the same cavity. This makes the attachment of the CSB's possible without any stresses being created in the boards by the steel plates. Consequently, counter sunk bolts were used for the hangers to have a flush finish on the steel plates at the bottom. The FCB (top), CSB (bottom) and CSB strips were then attached as shown in Fig. 4b.

2.3. Instrumentation and Loading

Multiple temperature measurements were taken during the test using K-Type Inconel sheathed thermocouples, which had a tip diameter of 1.5 mm. Six groups (G1-G6) of six thermocouples were placed along the SD system, with each group having the same thermocouple arrangement throughout the cross-section of the SD system as depicted in Fig. 5a. The structure was loaded using 40 kg sandbags (giving an average load of 1.56 kPa) placed uniformly on top of the SD system (which has a total weight of about 29.3 kN). The applied load corresponded to that of an office type occupancy building plus a partition load and factored using the Fire Limit State (FLS) load factor. Table 1 summarises the labelling convention of the thermocouple positions for easier understanding. Depending on the national code used, the FLS code be seen as a specific combination within the accidental limit state (i.e., ACC as per Eurocode and in South Africa), or as a separate limit state, and the term FLS simply refers to satisfy the associated test requirements, in this case outlined at the start of Sect. 2 above.

With the loading and instrumentation in place, the horizontal framing was boxed in using CSB on the sides and FCB on the top (see Figs. 5b and 6a). Furthermore, the CSB attached to the decking was extended to the outer furnace walls and sealed using a vermiculite mixture and covered with fibre ceramic blankets all round. Moreover, the columns were also protected using multiple layers of fibre ceramic blankets. The inside and outside of the final experimental setup is as depicted in Fig. 7. The burners were located along the east wall of the experimental setup.
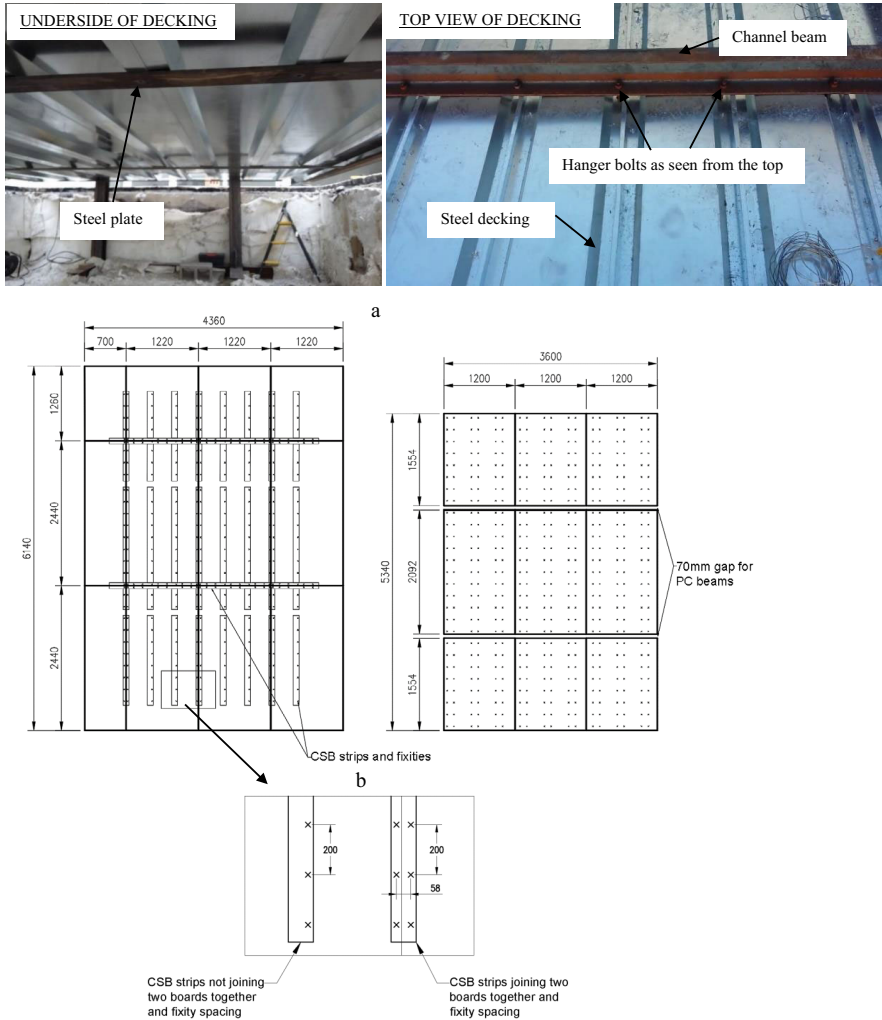
Figure. 4. (a) Steel plates used to attach VP50 decking to the bottom of the primary and tertiary beams and (b) layout and configuration of the fibre cement and calcium silicate boards.

3. Experimental Results

Figure 7 presents the average furnace temperature for the main furnace test in comparison to the ISO 834 standard fire curve. After an initial adjustment period of about three minutes, the furnace was able to produce the desired time–temperature curve. The test was run until 66 min, with a fire resistance of 60 min being desired for the system. The ambient temperature on the day of the test was around 9–10°C.
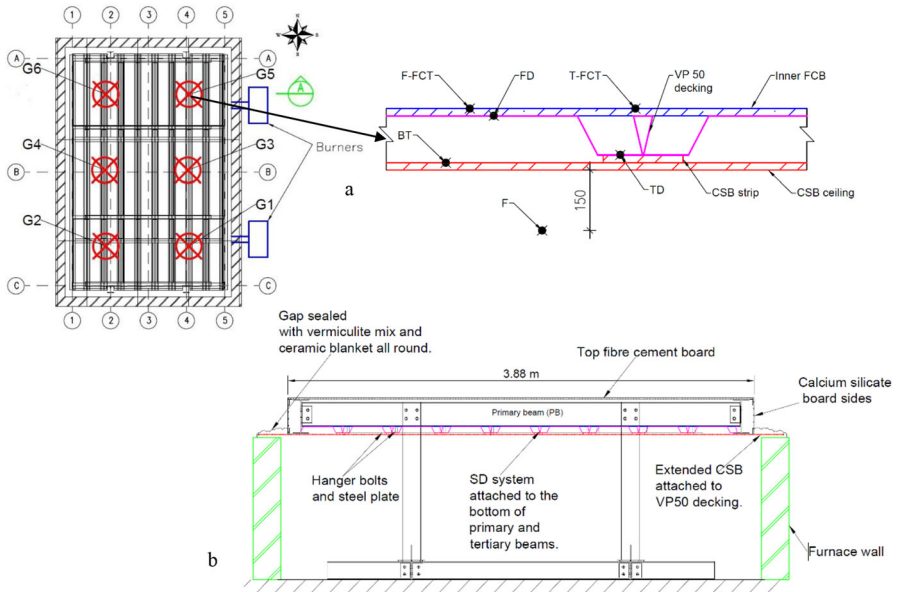
Figure. 5. (a) Layout and arrangement of thermocouple groups, **(b)** section view of experimental setup.

Table 1
Thermocouple Legend for Furnace Test

VP50-9 SD System Thermocouple Legend	Denotations
Calcium silicate **B**oard ceiling—**T**op	**BT**
Trough area—**T**op of steel **D**ecking,	**TD**
Flute area—**T**op of steel **D**ecking,	**FD**
Furnace gas	**F**
Flute area (Unexposed surface)—**T**op of **FCB**,	**F-FCT**
Trough area (Unexposed surface)—**T**op of **FCB**	**T-FCT**

Figure. 6. Aerial outside and inside view of the experimental setup.
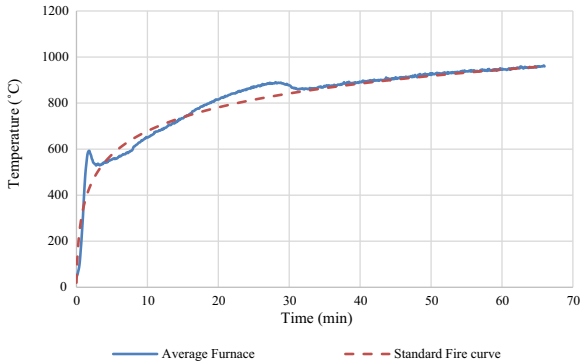
Figure. 7. Average furnace temperature in comparison to ISO 834 Standard Fire curve.

3.1. Test Observations and Temperature Profiles

The temperature profile through the layers of the decking system can be observed in Fig. 8, with the highest temperatures recorded at the top of the ceiling board (BT) locations, followed by the top of the decking at the flute (FD) and trough (TD) locations, and the lowest temperatures recorded at the top of the fibre cement boards at the flute (F-FCT) and trough (T-FCT) locations, as expected.

Starting with the BT locations, a rapid rise in temperature can be observed from the start of the test to a temperature of 100°C, followed by a halt in the temperature rise for a brief period, then a rise in temperature again consistent to the rise of temperature in the furnace. It took about 3.6 min on average to reach this temperature and lasted for about 4.4 min on average. This is due to the water content of the CSB reaching its boiling point and evaporating, with the additional latent heat energy required to evaporate the water from the boards halting the temperature rise. Visual observations of white smoke/steam began about 4 min into the experiment, which corresponds to the temperature data collected, and persisted for the majority of the experiment. At the end of the experiment, the highest temperature was recorded at G2 for this location, with a temperature of 695°C.

Moving on to the steel decking temperatures of the flute (FD) and trough (TD) locations, the temperatures for all FD locations are higher than that of the TD locations, with the exception of G2. This is in part due to the CSB strips running beneath the trough sections of the decking as shown in Fig. 3. The strips increase the distance and amount of material that the heat would need to conduct through to the subsequent top layer (i.e., the VP decking). This illustrates that the main mechanism of heat transfer through the system is by cavity radiation via the flute area, when compared to the conduction of heat through the boards and steel at the trough area, which is also consistent with the findings presented by Marx [23]. Furthermore, as stated by Marx [23], the shielding effect of the geometry of the steel at the trough area (TD locations) has an influence on the heat transfer through this section via cavity radiation as well, and thus expected to have lower
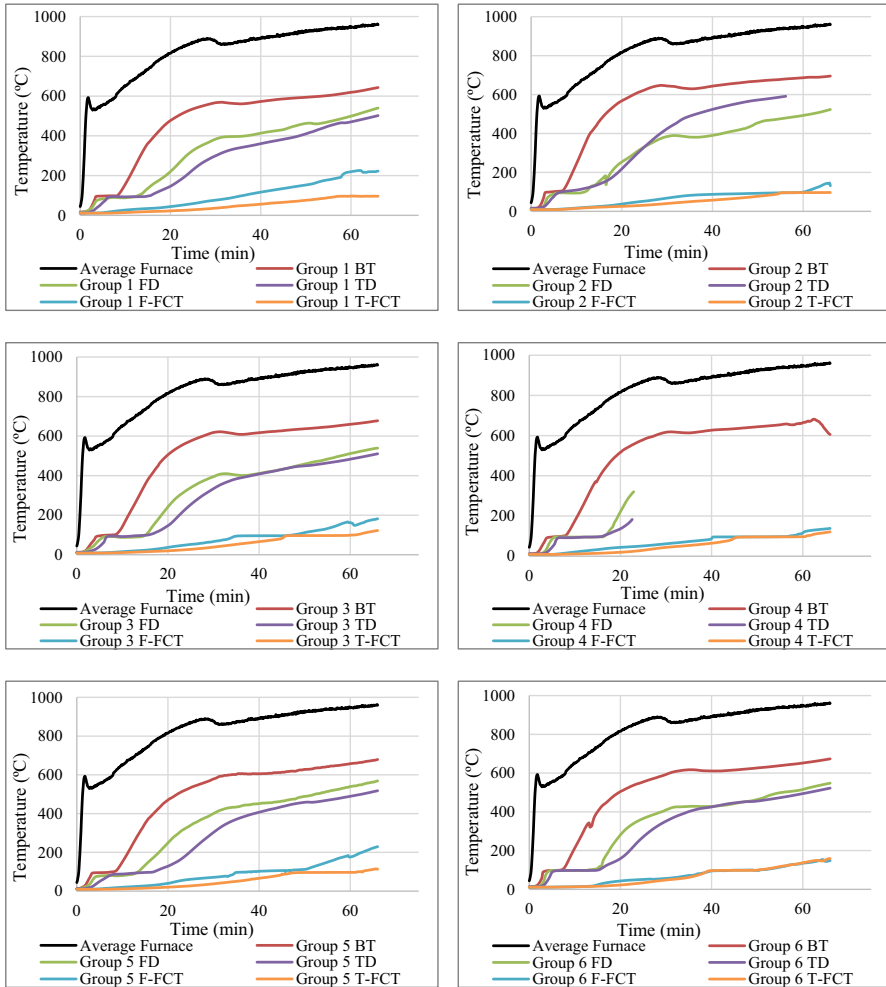
Figure. 8. Time–temperature curves captured from each of the group thermocouple locations. Where data is not listed, or stops, thermocouples were damaged. See Fig. 5a for the location of the groups. (Label convention as per Table 1: BT = CaSi Board Top; TD = Trough, top of Decking; FD = Flute, top of Decking; F-FCT = Flute, FCB Top; T-FCT = Trough, FCB Top.).

temperatures. This observation holds for all the groups except G2, where the temperatures within the trough was higher than that of the flute area. This was most likely caused by a small crack in the ceiling during testing. The maximum average temperature difference between the flute and trough area is 72.5%. The highest temperatures were recorded at G2 for the TD location with a temperature of 591°C at the 56th min, and G5 for the FD location with a temperature of 568°C at the end of the test.
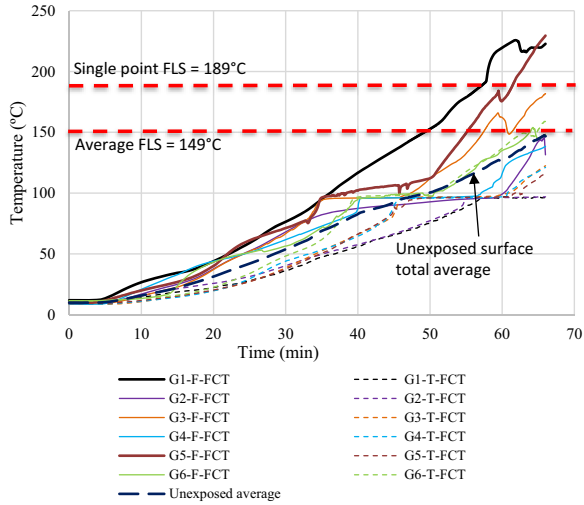
Figure. 9. Unexposed surface temperatures captured at the flute and trough area in comparison to the single point and average FLS temperatures. (Label convention as per Table 1: F-FCT = Flute, FCB Top; T-FCT = Trough, FCB Top.).

When considering the unexposed surface temperatures (T-FCT and F-FCT), the trough area location temperatures are all within the insulation FLS for the single point (180°C above ambient) and average temperature limits (140°C above ambient). Conversely, the average temperature of the flute area locations surpassed the FLS average temperature at the 59th minute and two single point locations surpassed the FLS single point temperature at the 57th and 61st minute. Furthermore, the total combined average temperature of the trough and flute areas measured are within the insulation FLS average temperature as indicated on Fig. 9. Thus, it can be concluded that the VP50-9 SD system does not meet the FLS insulation criteria for a 60-min fire rating, with a fire-rating of 57 min. As for the load bearing function and integrity FLS criteria, no structural failure of the decking system was observed during the experiment. Hence, it is safe to conclude the load bearing function criteria is met by the decking system.

No direct observations of the decking system could be made during the test as the system was enclosed, making the assessment of the decking system under the integrity criteria challenging. Upon inspection of the decking system after the load was removed, cracks were observed in the ceiling system and the FCB on top, but despite this the SD system was still intact as seen in Fig. 10a, b. Hence, it can be concluded that the assembly was able to keep its integrity for the entire duration of the tests and not let hot smoke or gasses pass through. Furthermore, the failure of the decking system according to the insulation FLS criteria occurred towards the end of the test. Hence, minor design changes can be implemented to mitigate this and will be discussed in the concluding section.
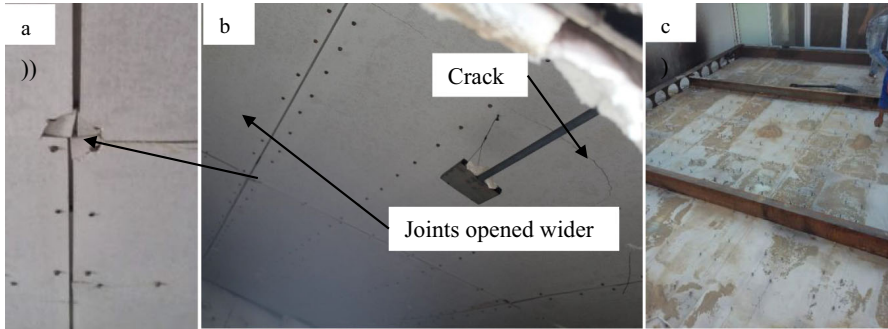
Figure. 10.   Ceiling system images after the test: (a) Enlarged view of failure at joint in ceiling, (b) underside of ceiling and (c) top of flooring system.

3.2. Collapse Observed in Preliminary Calibration Test

Before the main test conducted, as detailed above, a preliminary calibration test was performed in the furnace. Based on this preliminary test the furnace configuration, burner locations and chimney details were adjusted to improve performance. No steelwork was used and only the SD was placed over the top of the furnace, with temporary beams supporting the system at 1.925 m spacings.

At around the 18th minute of the test some of the furnace wall lining came loose and blocked the inlet from a burner. This appears to have directed hot burner gases directly onto the underside of the SD. A significant temperature rise on the unexposed face of the SD was observed from the 40th minute which was immediately followed by progressive collapse of the SD in this area, as shown in Fig. 11. It appears the ceiling system became damaged and allowed hot gases into the steel decking area. Even though the furnace temperature fell below the standard fire curve throughout this calibration test, the localised exposure of the SD above the burner is difficult to define but may have been severe and led to cracking of the ceiling board. Nevertheless, it highlights that once the ceiling is compromised the steelwork can rapidly heat up and cause structural collapse. This should be carefully considered in that the installation of lights, HVAC and other penetrations should be properly fire-stopped to prevent potential failure.

3.3. Numerical Model

The thermal behaviour of the SD system was further investigated using the Finite Element Method (FEM) and the temperature results from the experiment. The thermal model developed in this work is a representative section of the VP50-9 SD system. All components of the SD system have been included in the model, namely the fibre cement board (FCB), the VP50 profiled decking, the calcium silicate board (CSB) strips, and the CSB ceiling. With the heat transfer analyses performed, a better understanding of the governing parameters and governing modes of heat transfer is achieved, and thus, a more holistic understanding of the thermal response of the system. The model is compared to the average temperatures

Figure. 11. Failure at the South-West corner of the SD during the preliminary test.

from the same thermocouple locations obtained from each group (G1–G6) as shown in Fig. 8.

3.4. Model Parameters and Procedure

The model was developed using Abaqus version 6.17-1 [32]. Two physical constants were assigned for the Abaqus model attributes, namely the absolute temperature (− 273.15°C) and the Stefan-Boltzmann constant (5.67×10^{-8} W/m^{2}K^4). Two-dimensional (2-D) shell elements were used to model each of the VP-50-9 SD system components and assembled in the assembly module. The dimensions and geometry of the model is based on a 1640 mm wide section of the VP50-9 SD system, which includes four interlocked VP50 decking sheets. Solid homogeneous sections were assigned to each component, where their respective material properties were assigned.

A single transient heat transfer step was used in each of the analyses, with a time period of 3960 s, correlating to 66 min (i.e., the actual run time of the furnace test). An automatic increment procedure was used, with an initial and maximum increment size of 0.01 and 5 s, respectively. The maximum allowable temperature and emissivity change per increment was set to 10°C and 0.1, respectively. A pre-defined temperature field was assigned to the entire model in the initial step, with a temperature of 10°C, which corresponds to the ambient temperature recorded on the day of testing.

The same two-part heat transfer analysis procedure was followed in this work as a number of previous researchers considering similar configurations [18, 23, 33]. The average cavity temperatures were obtained and saved from the first analysis run which excludes the convective heat transfer within the cavities of the model. The saved time–temperature curves from the first analysis were then used as amplitudes to apply the convective heat transfer within the cavities as surface film conditions in the second analysis.
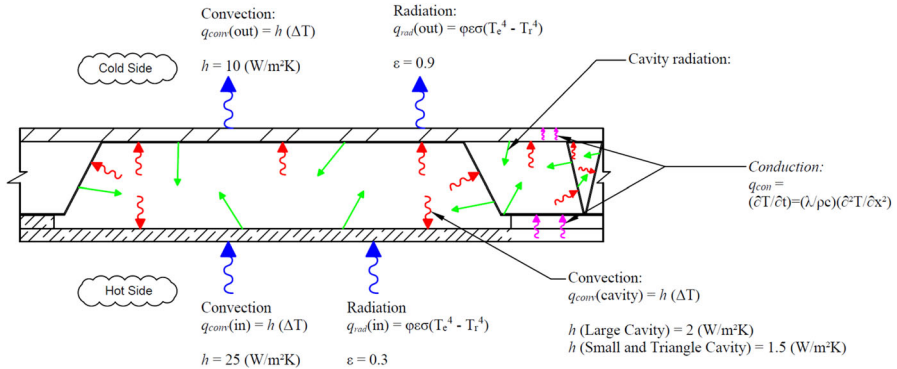
Figure. 12. Schematic of various heat transfer mechanisms considered in FE model.

Factors such as ventilation conditions, gas and flow properties make it difficult to measure the velocity within the furnace and the cavities of the SD system. As these parameters were unknown during testing, the exact values for the cavity convective heat transfer coefficients could not be determined [23]. A range (1 to 3 W/m^2K) of values were investigated in this work for the convective heat transfer coefficients used inside the cavities and are based on the relatively low values used in the previous validation studies and the work performed by Marx [23, 33, 34]. The preliminary results showed that the coefficients inside the cavities have a notable influence on the performance of the SD system. In essence, the higher the coefficient used, the more heat is transferred through the layers of the SD system as more heat is transferred within the cavities via convection. Three types of cavities have been defined in the model, namely the "Large cavity", which corresponds to the flute cavity area, the "Small cavity", which corresponds to the large cavity in the trough area, and the "Triangle cavity", which corresponds to the small triangular cavity in the trough area. The convective heat transfer coefficient for the large cavity was set to 2 W/m^2 K, and 1.5 W/m^2 K for the small and triangle cavity as these values yielded the best results as indicated in Figs. 12, 13 and 14.

3.5. Mesh and Interactions

A medium sized mesh was used to analyse the model, with a global seed size of 5 mm for the boards and strips, and split into three elements along the height of each board and strip component, resulting in an approximate mesh size of 3×5 mm. The VP decking was analysed with a global mesh size of 1×1 mm. Figure 15 depicts the mesh density used in this work and equates to 4594 elements. The 4-node linear heat transfer quadrilateral element type (DC2D4) was assigned to the model parts. The mesh size is based on the research conducted by Marx [23], who used a similar mesh density (global mesh of 5 mm for the boards and 1 mm for the decking) for this configuration, and found that using a smaller mesh size had a negligible change on the results. However, the mesh size used in
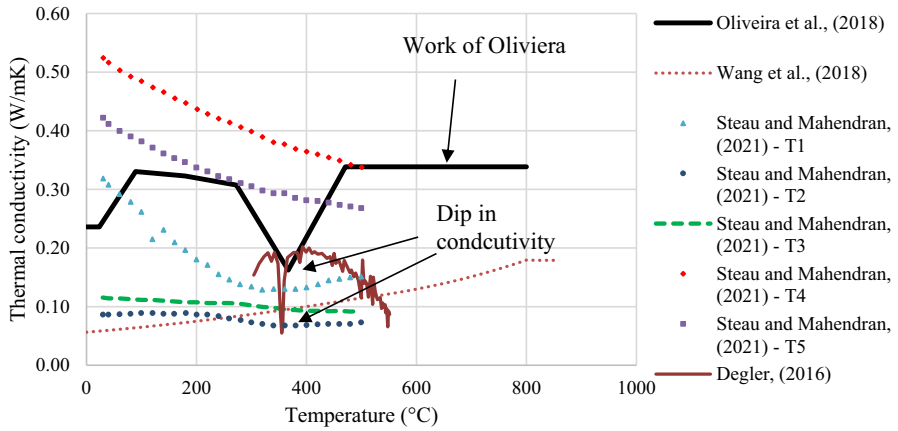
Figure. 13.   Temperature-dependent thermal conductivity values of Calcium Silicate Boards reported by various authors.
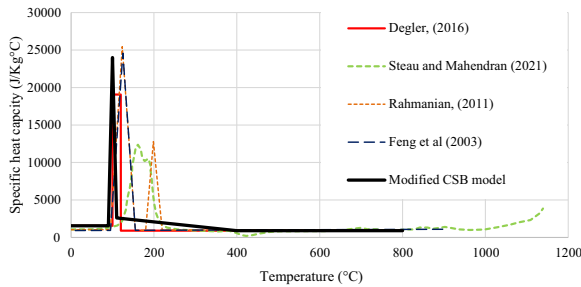

Figure. 14.   Specific heat capacity of Calcium Silicate Board.
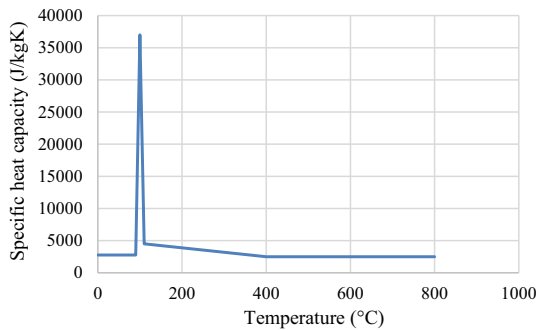

Figure. 15.   Modified specific heat capacity of Fibre cement board.

this study is slightly finer as the boards were split into three layers and not two as in the work conducted by Marx [23], such that the heat transfer through the board layers can be better captured.

Three interaction types were assigned in the thermal model, namely surface film conditions, surface radiation, and cavity radiation. The convective and radiative heat flux on the exposed side was defined with a surface film condition and surface radiation interaction, with a convective heat transfer coefficient (*h*) of 25 W/m^{2}K [23, 35]. A value of 0.3 has been used for the resultant emissivity of the furnace onto the ceiling to account for (a) emissivity of the furnace gases and walls, (b) emissivity of the CSB, and (c) to account for the depth of the furnace. Marx [23] used the same value, and based this value on the research conducted by Feng et al. [18]. These authors develop numerical models of similar sized cold-formed steel panel systems, using details from Shahbazian and Wang [36]. The average experimental furnace time–temperature curve measured in the experiment was used as an amplitude. The thermal boundary condition of the unexposed side was defined by a combined radiant and convective flux, with a convective heat transfer coefficient of 10 W/m^{2}K [18, 23], and an emissivity value of 0.9 [23], respectively.

Conduction between the interconnected layers was modelled using tie constraints. Ties equate the degrees of freedom of the surface nodes defined in the constraint. A total of three tie constraints were defined, linking the CSB to the CSB strips, the CSB strips to the VP decking bottom trough sections, and the VP decking flute top to the FCB. Abaqus provides the capability to model cavity radiation between the enclosed cavity surfaces. Only a single value for the emissivity is specified for each defined cavity. The same emissivity values implemented in previous work [23] have been used in this research. Marx [23] calculated the resultant emissivity of the CSB and the VP decking for the large cavity, and of the VP decking and the FCB for the small cavity. The resultant emissivity is calculated as described in [37].

3.6. Material Thermal Properties

The required thermal properties of the VP decking are assumed to be that of typical structural steel as detailed in [38], whilst the temperature-dependent emissivity of the VP decking was obtained from Marx (2018). The thermal conductivity (*λ*), specific heat capacity (*c*), and density (*ρ*) are considered for both the CSB and FCB.

3.7. Calcium Silicate Board

In the literature two studies have been identified [39, 40], where the temperature-dependent thermal conductivity (*λ*) and specific heat capacity (*c*) were determined for Promatec-H calcium silicate boards, which is the same material used in this study for the SD system. Oliveira [39] conducted a study to determine the temperature-dependent thermal conductivity of two types of calcium silicate boards, one of which was the Promatec-H calcium silicate board. Two experimental methods were investigated, namely the guarded hot plate and transient plane source theory (hot disk method). However, the data obtained from the guarded hot plate only has a temperature range of up to 40°C, and as a result only the data obtained from the hot disk method was implemented in this work. Figure 13 presents the temperature-dependent thermal conductivity values reported by various research-

ers of calcium silicate boards. Based on the similarity between the work by Oliveira [39] and the consistent results obtained relative to experimental data, the aforementioned material properties are incorporated in this work. The data obtained from Oliveira [39] is only given up until a temperature range of 470°C, thus, the last recorded conductivity was assumed constant for higher temperatures in this work.

Degler [40] conducted cone calorimeter tests to determine the temperature-dependent thermal conductivity of 6 Promatec-H calcium silicate board samples. Degler calculated the specific volumetric enthalpy (J/m^3) of the samples at four temperature intervals according to the formulation proposed by Wickstrom [41]. In short, the formulation proposed by Wickström allows for the addition of the latent heat required to model the chemical and physical phase changes that may occur within construction materials, such as dehydration reactions. The dehydration reactions that occur in the calcium silicate boards is assumed to be between the temperature interval of 100°C to 120°C only. The average volumetric enthalpy calculated for each temperature interval of the six tested samples by Degler [40] is implemented in this work. This was achieved by converting the volumetric enthalpy (J/m^3) to specific enthalpy (J/kg), by dividing throughout by the material density, then deriving the temperature-enthalpy curve to obtain the specific heat capacity as a function of temperature. However, the resulting temperature-dependent specific heat capacity increases suddenly (i.e., a step-wise function) where the dehydration reaction is assumed to occur. This characteristic, or shape, in specific heat capacity curve may cause convergence issues in the numerical analyses. Wang [42] proposed a solution to this by assuming a more gradual increase and decrease in specific heat capacity (triangular shaped) with a single peak value, but leaving the overall latent heat energy constant, which is adopted in this work.

The final shape of the specific heat capacity was obtained through a sensitivity analysis carried out in this work, where different triangular variations and peak specific heat capacity values were tested. Furthermore, it was identified through this sensitivity analysis that the total specific enthalpy change from 100 to 120°C (as in Degler [40] Fig. 13), which was calculated to be 381 MJ/Kg, was not sufficient to fully predict the dehydration process observed in the experimental data. Thus, the total enthalpy change within this temperature interval was multiplied by a factor of 1.32 (32% increase), equating to 503 MJ/Kg. This value increase is based on the data reported by [18, 43], who calculated similar extra latent heat energies in their respective models. Hence, this value increase is based on specific heat values for gypsum boards, however, given the similarities reported in literature for gypsum and calcium silicate boards, it was assumed to be similar in this work as well.

The modified specific heat capacity graph is presented below in Fig. 14 (referred to as modified CSB model), along with the originally derived specific heat capacity from Degler (2016), and the reported values from various other authors for gypsum and calcium silicate boards, including those mentioned above. A temperature interval of 90 to 110°C was assumed for the dehydration reaction to occur, with a peak value of 24 MJ/kg at 100°C. Additionally, a more gradual decrease in specific heat capacity between the temperature intervals of 110 to 400°C was assumed,

Table 2
Material Properties of Insulation Materials in FE Model

Material Name	Density (kg/m^3)	Conductivity (W/mK)	Specific heat (J/kgK)	Emissivity
Calcium silicate board	943 at 0°C 943 at 100°C 818 at 120°C 818 at 800°C	0.236 at 0°C 0.236 at 20°C 0.330 at 89°C 0.323 at 179°C 0.307 at 272°C 0.162 at 367°C 0.339 at 470°C 0.339 at 800°C	1727 at 10°C 1727 at 90°C 24,000 at 100 °C 2600 at 110°C 906 at 400°C 906 at 800°C	0.3
Fibre cement board	1250	0.25	2777 at 0°C 2777 at 90°C 37,000 at 100°C 4500 at 110°C 2500 at 400°C 2500 at 800°	0.9

with a maximum value of 2600 J/kg °C at 110°C. Care was taken not to alter the total amount of enthalpy change of 503 MJ/kg when assuming the shapes of the specific heat capacity Fig. 15.

The average wet and dry densities obtained by Degler [40] of the six tested samples was also implemented in this research. The final material properties of the calcium silicate board used in this study are as listed below in Table 2.

3.8. Fibre Cement Board

Very little data is reported in the literature on the temperature-dependent thermal properties of FCB. Hence, the thermal conductivity and density of the fibre cement board was obtained from the manufacture's technical data sheets [44]. Unfortunately, the manufacturer only supplies a single value for thermal conductivity, namely 0.25W/mK. However, it was found that the numerical solution provides satisfactory results based on this constant value. Similar to the conductivity, only a single density value of 1250 kg/m^3 was implemented in the numerical model, as supplied by the manufacturers.

A specific heat capacity of 2500 J/kgK was assumed initially, based on the research conducted by Marx [23]. However, Marx did not include the effects due to moisture in the numerical models. In this research, the specific heat capacity was modified according to the Wang (1995) formulation to account for the moisture content. The additional latent heat energy required for evaporation of the water can be obtained from (Eq – 1), where the latent heat of vaporisation of water is taken as 2.25 MJ/kg.

$$DCp = \frac{(2.25 \times 10^6)(u)}{\Delta T} * \Delta \tag{1}$$

where: *DCp* is the additional average specific heat (J/kg °C). *u* is the moisture content expressed as a fraction by weight. ΔT is the magnitude of the given temperature interval (°C) ∧ is a correction factor.

A moisture content of 15% was used in the formulation as supplied by the manufacturers. With a moisture content value of 15% and a correction factor of 1.9, equates to 641 MJ/kg calculated for the additional latent heat required for evaporation of the moisture. The correction factor ∧ is used to account for the required moisture evaporation–condensation migration under high pressure as stated by Wang (1995), and other endothermic chemical reactions that may occur within this temperature interval that has not been accounted for. Approximately 45% of this extra energy was distributed over a temperature range of 290°C, from 110°C to 400°C, similar to that of the CSB. The remainder of the energy was distributed between the temperature range of 90°C and 110°C, with a peak specific heat capacity value of 37 MJ/kgK at 100°C. Finally, it was also identified during the preliminary modelling stage that using a specific heat capacity of 2777 J/kgK instead of 2500 J/kgK, in the temperature range of 0 to 90°C provided better correlation with the experimental data. The final thermal properties of the boards implemented in this work are listed in Table 2.

3.9. *Numerical model results and comparison*

This section discusses the predicted and experimental temperatures obtained for the SD system. The temperature point selected from the FEM model corresponds to the temperature locations measured in the experiment. The T-FCT (unexposed surface temperature at the trough area) experimental data was compared to that of the average temperatures obtained from the node locations depicted in Fig. 16. The various final temperature distributions can also be seen in Fig. 17.

Figure 17 depicts the average temperatures from the same locations of each group (G1-G6), which includes error bars such that the range of experimental data can be visualized, and compared to the FEM analysis results. Overall trends are captured well and there is good agreement between the results, especially in the lower sections of the system. Upper temperatures are slightly over-predicted, especially after 40 min.

The model was able to predict the temperature evolution of the top of the ceiling board (BT) location to a reasonable degree, with an error difference of less than 10.5% from the 20th minute to the end of the test, and an error difference of only 2.1% in the final temperature. However, the model slightly under-predicts the dehydration reaction period that occurred in the calcium silicate boards in the experiment. When comparing the assumed temperature intervals of 90 to 110°C at this location, the experimental data experienced a longer dehydration period of about 4.4 min, from 3.6 to 8 min into the test. The dehydration period predicted by the model only lasts about 2.2 min, from 4.3 to 6.6 min into the model analysis. After the dehydration period is completed, the model tends to over-predict the temperature evolution of the calcium silicate board. However, the rise in temperature is consistent to the rise in temperature of the experimental data, which is a result of the assumed gradual decrease in the specific heat capacity from a temper-
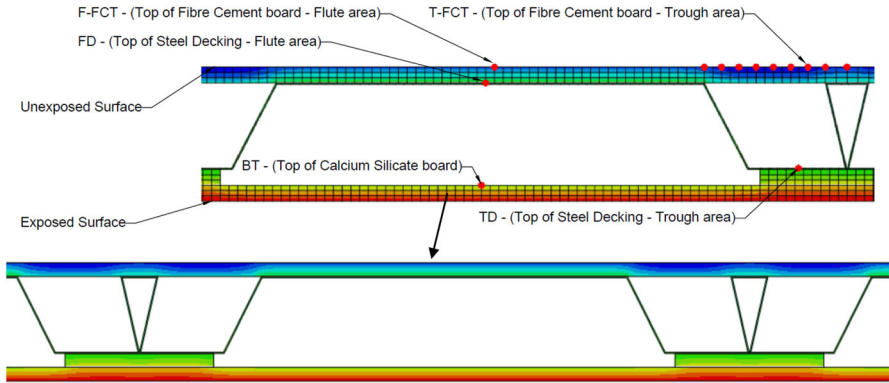
Figure. 16.   Node locations used to obtain final predicated temperatures and final predicated temperature profile.
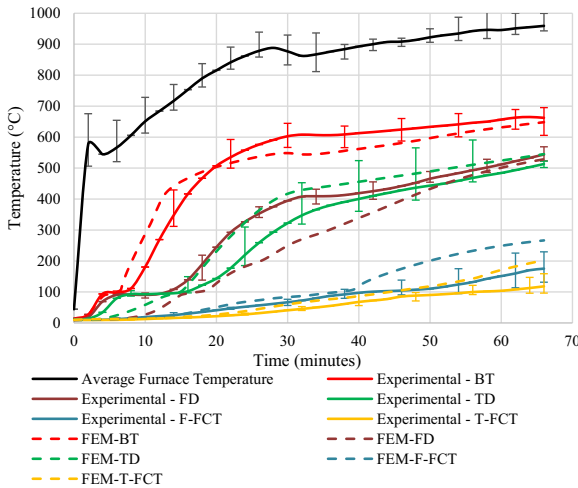

Figure. 17.   Finite Element Model results compared to the experimental average group temperatures from the same thermocouple locations.

ature of 110 to 400°C of the calcium silicate board as detailed above. This continues until a temperature of about 500°C is reached where the model starts to under predict the experimental data at about the 19-min mark.

When considering the top of the steel decking at the trough (TD) and flute (FD) temperature locations, there is a noticeable difference in the behaviour of the model and the experimental data. The predicted temperature evolution has a slower increase in temperature during the start of the analysis for the TD location, and consistently under-predicts the temperature evolution at the FD location. The error difference is especially evident for the FD location. This behaviour also occurred in the heat transfer models developed by Marx [23] and is not well

understood. However as stated by Marx [23], it is possible that the increase in temperature of the bottom part of the VP decking could have caused the steel profile to experience thermal bowing, resulting in small openings being formed between the interconnected sheets, thereby allowing more heat to be transferred to the upper layers through convection and radiation for the FD location in the actual experiment. However, when compared to the experimental data, the model temperatures at these two locations converge to similar final temperatures, with an error difference of 6.2% and 2.8% for the FD and TD locations, respectively.

An important result to note is that the predicted and experimental steel temperatures are around 500°C at 60 min. For such temperatures Eurocode EN 3-1-2 typically estimates that steel loses around 22% of its strength and 40% of its stiffness. Due to the fire limit state load factors this will typically be sufficient to carry the reduced loads and maintain structural resistance. Local buckling of the steelwork was not noted after the experiment, and appears to have been prevented by the fixings and boards.

When considering the unexposed surface temperatures at the top of the FCB at the trough (F-FCT) location, the model was able to predict the recorded temperatures well up until the 40th minute mark, where the predicted temperatures start to increase at a more rapid rate and diverge from the experimental data. This discrepancy is may be attributed to many factors, including (a) the lack of material data on the FCB, (b) deformations causing reduced contact between elements leading to lower levels of conduction, and (c) the presence of sandbags on top of the FCB in the experimental setup, which could have acted as a heatsink, thus lowering the temperatures measured in the experiment. The sandbags contained commercially supplied sand that was slightly moist. Hence, these are likely to have provided a medium to conduct heat away from the surface whilst also providing cooling from the moisture content. In a real-world application the loads would rather be applied by the suspended computer flooring, resulting in a mostly empty void. For predictive models below the influence of the sandbags has been neglected as they would provide a non-conservative fire rating, in terms of insulation. Hence, the work rather seeks to provide lower-bound numerical estimates of the fire rating.

The error difference in the final temperatures predicted at this location is 52%. Similarly to the F-FCT location, the model was able to predict the temperature evolution of the of the top of the FCB at the trough (T-FCT) location well up until about the 50th minute into the analysis, where the model temperatures also start to increase at a more rapid rate. The error difference in the final temperatures predicted is 71% with a temperature difference of 84°C.

Furthermore, the numerical model also indicates that the main mechanism of heat transfer within the SD system is via cavity radiation in the flute area, as the unexposed temperatures of the flute section are higher than that of the trough section, similar to the results recorded in the experiment. Lastly, when comparing the unexposed surface numerical results to the FLS average and single point limit temperatures of 149°C and 189°C, respectively, the FEM-T-FCT and FEM-F-FCT temperatures surpass both the average and single point temperatures at the 56th and 63rd minute mark, and at the 42nd and 48th minute mark, respectively.

Thus, the estimated fire resistance rating for the VP50-9 SD system calculated by the model is 42 min. This is lower than the experimental value of 57 min, but the lower bound numerical estimate has been maintained to primarily neglect the effect of the sandbags on the top surface.

4. Discussion and Conclusions

This paper has provided experimental and numerical data on a novel sandwich decking (SD) structural system incorporating a calcium silicate ceiling (CSB), continuous steel decking and a fibre cement board (FCB) trafficable floor. This system could potentially be used as an innovative flooring system in a wide variety of industries due to the ease of construction, lack of wet work, limited skills and equipment needed by installers and a suitable fire rating. However, acoustic performance may need to be enhanced depending on requirements.

Past work on the SD has lacked large-scale experimental data, especially that incorporating loaded samples at elevated temperatures, leading to uncertainties regarding its resistance and behaviour. The large-scale experimental test showed that integrity and structural resistance were maintained throughout a 60-min standard fire test. Insulation resistance requirements were exceeded at around 57 min. Minor cracking occurred across the CSB, with extensive cracking on the top FCB.

The steel decking, which provides a significant proportion of the structural resistance, attained a temperature of around 500°C in both the numerical model and experimental test at 60 min. Based on typical material reduction factors it appears that structural strength will still be sufficient, consistent with fact that structural resistance was maintained throughout the test.

Numerical models provide consistent predictions for the majority of positions. However, differences are observed at the top of the FCB and inner cavity locations. As noted above, it is believed this difference is influenced by the presence of the sandbags acting as a heatsink, moisture in the sandbags, the deformation of the decking leading to changing interactions, and uncertainty in material properties at elevated temperatures. Further research is required to quantify these effects. Numerical models have indicated a lower insulation resistance rating of around 42 min, providing a more conservative estimate of performance. It was not physically possible to load the sample in a different way, but further work should rather base the estimated insulation resistance on the lower value until further information is available. Also, changes in connectivity between elements over time should be considered and the extent to which it influence heat transfer.

A number of recommendations are proposed for enhancing the system:

– Utilising a 12 mm or 20 mm FCB for the floor surface. This will significantly improve the insulation and structural resistance of the SD. Also, based on conversations with contractors it has been identified that the 9 mm board may be susceptible to punching from point loads. Hence, both fire and practical considerations can be addressed through this modification.

– In a preliminary calibration test, structural collapse was observed after the ceiling was damaged, and hot gases penetrated the plenum and heated up the steel decking. This highlights the need to firestop any penetrations in the system.
– In Fig. 4 it shows how the decking is continuous under support beams, but the FCB is cut at the position of supporting steel channels. This may lead to the channels becoming heated based on measured temperatures at the underside of the FCB. It is proposed that the FCB should rather be continued underneath support beams to provide additional insulation.

Acknowledgements

Funding

Declarations

Conflict of interest The authors declare no conflict of interest

Open Access

References

1. Wright HD, Evans HR, Burt CA (1989) Profiled steel sheet/dry boarding composite floors. Struct Eng A 67:114–120
2. Jahan A (2018) Axial and shear behavior of profiled steel sheet dry board (Pssdb) composite walling system
3. Awang H, Badaruzzaman W (2011) Development of profiled steel sheeting dry board roof panel system in school classroom modules. J Civ Eng Constr Technol 2:72–81
4. Badaruzzaman W, Ahmed E, Rashid A (1996) Behaviour of profiled steel sheet dry board system. In: Beijing International Conference, pp 21–24
5. Wan Badaruzzaman WH, Zain MFM, Akhand AM, Ahmed E (2003) Dry boards as load bearing element in the profiled steel sheet dry board floor panel system—structural performance and applications. Constr Build Mater 17:289–297. https://doi.org/10.1016/S0950-0618(02)00105-8
6. Awang H, Nordin N, Wan Badaruzzaman WH (2009) The application of profiled steel sheeting dry board (Pssdb) industrialised building system
7. Gillie M, Usmani AS, Rotter JM (2001) A structural analysis of the Cardington British steel corner test. J Constr Steel Res 58:427–442
8. Seif M, Main J, Weigand J, McAllister TP, Luecke W (2016) Finite element modeling of structural steel component failure at elevated temperatures. Structures 6:134–145. https://doi.org/10.1016/j.istruc.2016.03.002
9. Al-Jabri KS, Burgess IW, Lennon T, Plank RJ (2005) Moment–rotation–temperature curves for semi-rigid joints. J Constr Steel Res 61:281–303. https://doi.org/10.1016/j.jcsr.2004.09.001
10. Walls RS, Viljoen C, de Clercq H (2018) Analysis of structures in fire as simplified skeletal frames using a customised beam finite element. Fire Technol 54:1655–1682. https://doi.org/10.1007/s10694-018-0762-7
11. LaMalva K, Hopkin D (2021) International handbook of structural fire engineering. Springer, Cham. 10.1007/978-3-030-77123-2
12. Hurley MJ, Gottuk D, Hall JR, Harada K, Kuligowski E, Puchovsky M, Torero JL, Watts JM Jr, Wieczorek CJ (2016) SFPE handbook of fire protection engineering, 5th edn. Springer, New York
13. Walls RS, Viljoen C, de Clercq H, Clifton GC (2017) Reliability analysis of the slab panel method (SPM) for the design of composite steel floors in severe fires. J Struct Fire Eng 8:84–103. https://doi.org/10.1108/JSFE-01-2017-0008
14. Clifton G, Meng F, Andisheh K, Kordani R (2022) The slab panel method: design of composite floor systems for severe fires, HERA report R4–131 2022 edition. New Zealand Heavy Engineering Research Association, Manukau City
15. Bisby L, Gales J, Maluk C (2013) A contemporary review of large-scale non-standard structural fire testing. Fire Sci Rev 2:1–27. https://doi.org/10.1186/2193-0414-2-1
16. Gales J, Maluk C, Bisby L (2012) Large-scale structural fire testing—how did we get here, Where are we, and where are we going? In: 15th Int Conf Exp Mech. Fire Symp, pp 1–22
17. O'Loughlin E, Lay S (2015) Structural fire resistance: rating system manifests crude, inconsistent design. Case Stud Fire Saf 3:36–43. https://doi.org/10.1016/j.csfs.2015.03.001
18. Feng M, Wang Y, Davies J (2003) Thermal performance of cold-formed thin-walled steel panel systems in fire. Fire Saf J 38:365–394. https://doi.org/10.1016/S0379-7112(02)00090-5

19. Chen W, Ye J, Bai Y, Zhao XL (2012) Full-scale fire experiments on load-bearing cold-formed steel walls lined with different panels. J Constr Steel Res 79:242–254. https://doi.org/10.1016/j.jcsr.2012.07.031

20. Ariyanayagam AD, Mahendran M (2017) Fire tests of non-load bearing light gauge steel frame walls lined with calcium silicate boards and gypsum plasterboards. Thin-Walled Struct 115:86–99. https://doi.org/10.1016/j.tws.2017.02.005

21. Steau E, Mahendran M, Poologanathan K (2020) Experimental study of fire resistant board configurations under standard fire conditions. Fire Saf J . https://doi.org/10.1016/j.firesaf.2020.103153

22. Steau E, Mahendran M (2020) Thermal modelling of LSF floor-ceiling systems with varying configurations. Fire Saf J . https://doi.org/10.1016/j.firesaf.2020.103227

23. Marx H (2018) Thermal behaviour of a novel cellular beam structural system in fire. Stellenbosch University, Stellenbosch

24. Marx H, Walls R (2019) Thermal behaviour of a novel non-composite cellular beam floor system in fire. J Struct Fire Eng 10:354–372. https://doi.org/10.1108/JSFE-10-2018-0032

25. Kloos M (2017) An investigation into the structural behaviour of a novel cellular beam structure in fire. Stellenbosch University, Stellenbosch

26. Kloos M, Walls RS (2019) Finite element modelling of the structural behaviour of a novel cellular beam non-composite steel structure in fire. Int J Steel Struct . https://doi.org/10.1007/s13296-019-00215-5

27. Claasen J, Walls RS, Cicione A (2021) figshare: My data, Stellenbosch Univ. https://doi.org/10.6084/m9.figshare.16940824

28. Claasen J (2022) Experimental testing and numerical modelling of a large-scale modular cellular structural steel and composite sandwich decking flooring system in fire. Stellenbosch University, Stellenbosch

29. Claasen J, Walls R, Cicione A, Streicher D (2022) Structural behaviour of a novel modular cellular steel beam system at elevated temperatures based on large-scale experimental testing and numerical modelling. J Constr Steel Res . https://doi.org/10.1016/j.jcsr.2022.107512

30. Ignis Testing (2021) Ignis testing—fire resistance testing laboratory—Cape Town

31. SABS, Sans 10177-2:2005 (2005) Fire testing of materials, components and elements used in buildings. Part 2: fire resistance test for building elements. SABS, Pretoria

32. Dassault Systemes (2016) Abaqus 2016 documentation. Dassault Systemes Simulia Corporation

33. Jeffers A, Wickstrom U, McGrattan K. Documentation of the solutions to the SFPE heat transfer verification cases

34. Wickström U, Palsson J (1999) A scheme for verification of computer codes for calculating temperature in fire exposed structures. Fire Technol 36:31

35. BSI (2002) Eurocode 1: actions on structures—part 1–2: general actions—actions on structures exposed to fire. British Standards Institute, London

36. Shahbazian A, Wang YC (2013) A simplified approach for calculating temperatures in axially loaded cold-formed thin-walled steel studs in wall panel assemblies exposed to fire from one side. Thin-Walled Struct 64:60–72. https://doi.org/10.1016/j.tws.2012.12.005

37. Buchanan AH, Abu AK (2017) Structural design for fire safety, 2nd edn. Wiley, Cantebury

38. BSI (2005) EN 1993-1-2: Eurocode 3: design of steel structures—part 1–2: general rules—structural fire design. Britisch Standard Institute, London

39. De Oliveira TB, Alves TA, Mesquita LMR (2018) Thermal conductivity of calcium silicate boards at hight temperatuers: an experimental approach. In: Proc 1st Iber Conf Theor Exp Mech Mater/11th Natl Congr Exp Mech, pp 171–182
40. Degler J (2016) Determination of the conductivity of insulation boards made of calcium silicate by test in the cone calorimeter. Luleå University of Technology, Luleå
41. Wickstrom U (2016) Temperature calculation in fire safety engineering. Springer, Cham
42. Wang H-B (1995) Heat transfer analysis of components of construction exposed to fire. University of Salford, Salford
43. Rahmanian I (2011) Thermal and mechanical properties of gypsum boards and their influences on fire resistance of gypsum board based systems, p 252
44. ETEX Group (2020) Kalsi partition technical data sheet